Journal of Colloid and Interface Science **248,** 176–184 (2002)
doi:10.1006/jcis.2001.8200, available online at http://www.idealibrary.com on IDEAL®

Electrokinetic Flow through an Elliptical Microchannel: Effects of Aspect Ratio and Electrical Boundary Conditions

Jyh-Ping Hsu,*,[1] Chen-Yuan Kao,* Shiojenn Tseng,† and Chur-Jen Chen‡

*Department of Chemical Engineering, National Taiwan University, Taipei, Taiwan 10617, Republic of China; †Department of Mathematics, Tamkang University, Tamsui, Taipei 25137, Republic of China; and ‡Department of Mathematics, Tunghai University, Taichung, Taiwan 403, Republic of China

Received September 19, 2001; accepted December 20, 2001; published online February 21, 2002

The electrokinetic flow of an electrolyte solution through an elliptical microchannel is studied theoretically. The system under consideration simulates the flow of a fluid, for example, in vein. We show that, for a constant cross-sectional area, both the electroosmotic volumetric flow rate and the streaming potential increase monotonically with an increase in the aspect ratio, and both the total electric current and the electroviscous effect may exhibit a local minimum as the aspect ratio varies. Also, for a constant average potential on the channel wall, the difference between the results based on three kinds of boundary conditions, which include constant surface charge, constant surface potential, and charge-regulated surface, is inappreciable if the hydraulic diameter is larger than 1 μm.

Key Words: **electrokinetic phenomenon; elliptical microchannel; aspect ratio; electroosmotic flow; electroviscous effect.**

I. INTRODUCTION

Electrokinetic phenomena, for example, electrophoresis and electroosmosis, play an important role in many fields of practical significance. Although relevant studies are ample in the literature, available results for electrokinetic flow in a microchannel are relatively limited, and the topic has drawn the attention of researchers only recently. This is mainly due to the fact that the operating parameters, such as friction factor and pressure gradient, have a strong influence on the behavior of flow field (compare with the conventional transport theories) in micrometer or submicrometer scale vessels. Recent improvement in both material science and manufacturing technology makes the application of fluid flow in a microchannel more versatile and attractive. Typical examples in this area include microchannel heat sinks for cooling microchips, microreactors for modification and separation of biological cells, flow through filter cakes and synthetic membranes (which may have capillary pores), and micro fluid pumps. Apparently, it is highly desirable to a have a more accurate description of the fundamental characteristics of the flow system. Burgreen and Nakache (1) analyzed the electrokinetic flow in an ultrafine capillary slit by extending the classic theory, which is limited to the flow in a channel of large electrokinetic radius or to an interface at low surface potentials. Rice and Whitehead (2) investigated the effect of electrokinetic radius on the behavior of the electrokinetic phenomena in a narrow cylindrical capillary under the Debye–Hückel condition (i.e., low electrical potential). Sørensen and Koefoed (3) evaluated the electrokinetic phenomenological coefficients for capillaries with a circular cross section under the Debye–Hückel condition at all ratios between pore radius and Debye length. Bowen and Jenner (4) discussed the electroviscous effects in a charged capillary. A numerical solution for the Poisson–Boltzmann equation describing the electrical potential distribution was developed, and they concluded that the mobility of ions of signs opposite to those on the capillary wall has a strong dependence on electroviscous effects. Mala *et al*. (5) studied theoretically the effect of an electrical double layer on both liquid flow and heat transfer in the case of a planar slit at constant temperature under the Debye–Hückel condition. They conclude that both the volumetric flow rate and the heat transfer capacity will be overestimated if the effect of the electrical double layer is neglected. Qian *et al*. (6) proposed a numerical algorithm to obtain the electrical potential distribution in a charged capillary filled with arbitrary electrolytes by introducing a Poisson–Boltzmann integral equation, which was derived from the physical principles for electrostatic fields and thermodynamic systems. Mala *et al*. (7) studied experimentally the effects of an electrical double layer on flow characteristics with different KCI concentrations in water and different plate materials in the case of a planar slit. A mathematical model, which took the presence of the electrical double layer into account, was also developed under the Debye–Hückel condition. They found that the predicted volumetric flow rates agree well with the measured data. A two-dimensional problem in which an electrolyte solution flows through a rectangular microchannel was considered by Mala *et al*. (8). Both an analytical result based on the Debye–Hückel approximation and the corresponding exact numerical values were presented. They showed that the former might significantly overestimate the electrical potential near the channel wall and in the corner regions. Yang and Li (9, 10) considered the problem of a pressure-driven flow of an electrolyte solution

[1] To whom correspondence should be addressed. Fax: 886-2-23623040. E-mail: jphsu@ccms.ntu.edu.tw.

0021-9797/02 $35.00

in a rectangular microchannel. A two-dimensional electric field was solved both numerically (9) and analytically (10) under the Debye–Hückel condition, and a Green function approach was adopted to solve the flow field. They showed that the apparent viscosity strongly depends on the electrokinetic diameter, the ionic concentration, and the zeta potential of the channel wall. The flow and heat transfer characteristics in rectangular microchannels with and without consideration of the electrokinetic effects were theoretically evaluated by Yang *et al*. (11) and Mala and Li (12), and Weilin *et al*. (13) studied experimentally the characteristics of the flow of deionized water in both microtubes and trapezoidal silicon microchannels. Their results all revealed a significant difference in pressure gradient compared to that predicted by conventional laminar flow theory for smaller dimension channels. Huisman *et al*. (14, 15) investigated both experimentally and theoretically various electrokinetic methods to characterize ultrafiltration membranes, which contain cylindrical pores with a diameter on the order of 10 nm. Ren *et al*. (16) examined the electroviscous effects on liquid flow in a rectangular microchannel. A comparison between the experimental data gathered by them and an electrokinetic flow model derived revealed that the presence of an electrical double layer is the major cause for the significantly higher pressure drop for pure water and dilute aqueous ionic solutions flowing through small microchannels. Kemery *et al*. (17) studied experimentally the transport behavior induced by an applied electric field in nanometer-sized channels. Nanoporous polycarbonate nuclear-track-etched membranes with highly monodispersed pores with an average diameter of 15 nm were used. Coelho *et al*. (18) investigated theoretically the electroosmotic phenomenon in a porous media; the linearized electrokinetic equations were solved and various geometries were considered.

The previous discussions reveal that most of the relevant studies in the literature are limited to some simple geometry or trapezoidal cross section. Also, drastic assumptions are made so that mathematical analysis can be simplified, and an analytical result can be derived. Unfortunately, the cross section of microchannels used in practice may assume various shapes. Blood capillary and lymphatic microchannels, for instance, will deform when they experience pressure from surrounding muscle. This suggests that a geometry more flexible than those assumed previously should be considered. To this end, a channel with an elliptical cross section seems to be an appropriate choice since it can simulate various geometries by adjusting its shape parameters. The present study investigates theoretically the electrokinetic flow in an elliptical microchannel under three types of surface conditions. No assumptions are made regarding the thickness of the double layer and the level of the electrical potential. The present study extends previous analyses to a more general case and a more realistic description for biological systems.

II. THEORY

Referring to Fig. 1a, we consider a steady flow of an incompressible $a : b$ electrolyte solution in an elliptical microchannel

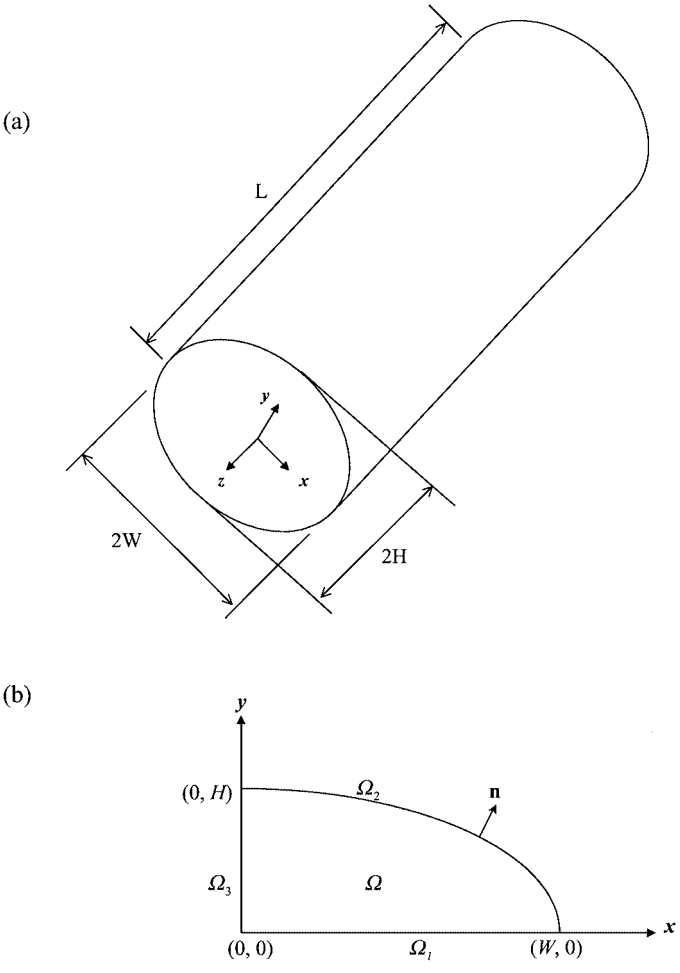

FIG. 1. A schematic representation of the problem considered. (a) $2W$, $2H$, and L are, respectively, the length of the major axis, the length of the minor axis, and the length of the elliptical microchannel. (b) The computational domain has cross section Ω, and its boundary comprises Ω_1, Ω_2, and Ω_3.

with major axis $2W$, minor axis $2H$, and length L. Suppose that L is sufficiently large so that the end effect of the flow phenomenon is negligible. The Cartesian coordinates are chosen with its origin located at the center of the microchannel, and the flow of liquid is in the z direction. This implies that both the x and the y components of the fluid velocity V vanish. Suppose that the z component of V, V_z, is a function of x and y, which is expressed as $V_z = u(x, y)$. A uniform electrical field, E_z with strength $E_z = -\partial\psi/\partial z$, and a uniform pressure gradient, P, with magnitude $P = -\partial p/\partial z$, are applied in the z direction, ψ and p being, respectively, the electrical potential and the pressure. The dielectric constant and the viscosity of the liquid phase are denoted by ε and η, respectively, and both are assumed to be constant. Referring to Fig. 1b, the symmetric nature of the problem suggests that only the quarter domain of the elliptical cross section, $\Omega \in [x^2/W^2 + y^2/H^2 \le 1 \cap x \ge 0 \cap y \ge 0]$, the boundary of which comprises Ω_1, Ω_2, and Ω_3, needs to be considered.

II.1. Electrical Field

The electrical potential $\psi(x, y, z)$ comprises that due to the applied electrical field, $-E_z z$, and that due to the charged surface, $\phi(x, y)$. Suppose that $\psi(x, y, z)$ can be expressed as (19)

$$\psi(x, y, z) = \phi(x, y) - E_z z. \quad [1]$$

We assume that $\phi(x, y)$ can be described by the Poisson equation

$$\frac{\partial^2 \phi}{\partial x^2} + \frac{\partial^2 \phi}{\partial y^2} = \frac{-\rho}{\varepsilon}, \quad (x, y) \in \Omega, \quad [2]$$

where ρ is the space charge density. If the concentrations of ionic species in the solution follow the Boltzmann distribution, then

$$\rho = -aC_a^0 F[\exp(bF\phi/RT) - \exp(-aF\phi/RT)], \quad [3]$$

where a and b are the valences of cations and anions, respectively, T is the absolute temperature, and R and F are, respectively, the gas constant and the Faraday constant. In the following discussions the subscript a (b) represents the properties of cations (anions) and the superscript 0 denotes the bulk properties. For instance, if C is the concentration, then C_a^0 represents the bulk concentration of cations. Equation [2] can be rewritten in scaled form as

$$\frac{\partial^2 \Phi}{\partial X^2} + \frac{\partial^2 \Phi}{\partial Y^2} = \frac{K^2 G}{a + b}, \quad [4]$$

where $\Phi = F\phi/RT$, $G = \exp(b\Phi) - \exp(-a\Phi)$, $X = x/D_h$, $Y = y/D_h$, and $K = kD_h$. $D_h = \pi H / \int_0^{\pi/2} \sqrt{1 - [1 - (H/W)^2] \sin^2 \theta}\, d\theta$ is the hydraulic diameter of the elliptical microchannel (20), and the Debye–Hückel parameter k is defined by

$$k = \left(\frac{aC_a^0 (a + b) F^2}{\varepsilon RT} \right)^{1/2} = \left(\frac{2IF^2}{\varepsilon RT} \right)^{1/2}, \quad [5]$$

$I = a(a + b)C_a^0/2$ being the ionic strength.

II.2. Boundary Conditions

Two of the boundary conditions associated with Eq. [4] arise from the symmetric nature of the problem under consideration. We have

$$\nabla\Phi \cdot n = 0, \quad (x, y) \in \Omega_1 \text{ or } \Omega_3. \quad [6]$$

Three types of channel walls are considered: (a) constant surface potential, (b) constant surface charge density, and (c) charge-regulated surface. The boundary conditions associated with Eq. [4] for cases (a) and (b) can be expressed, respectively, as

$$\Phi = \Phi_0, \quad (x, y) \in \Omega_2 \quad [7]$$

and

$$\nabla\Phi \cdot n = \Gamma, \quad (x, y) \in \Omega_2. \quad [8]$$

In these expressions, ∇ is the scaled gradient operator, n is the unit outer normal vector at boundaries, as shown in Fig. 1b, $\Gamma = \sigma D_h F/\varepsilon RT$, and σ is the surface charge density on Ω_2. For case (c) we assume that the simple one-site dissociation reaction below occurs on the channel wall:

$$AH \Leftrightarrow A^- + H^+. \quad [9]$$

Let K_d be the dissociation constant defined by

$$K_d = \frac{C_{A^-}^{\Omega_2} C_{H^+}}{C_{AH}^{\Omega_2}}, \quad [10]$$

where the superscript Ω_2 represents the surface properties on the channel wall. Suppose that the space distribution of H^+ follows the Boltzmann distribution; that is,

$$C_{H^+} = C_{H^+}^0 \exp(-\Phi). \quad [11]$$

If we let N_s be the sum of the concentration of A^- and that of AH, that is,

$$N_s = C_{A^-}^{\Omega_2} + C_{AH}^{\Omega_2}, \quad [12]$$

Eqs. [10]–[12] lead to

$$C_{A^-}^{\Omega_2} = \frac{N_s}{1 + \left(C_{H^+}^0/K_d\right) \exp(-\Phi)}. \quad [13]$$

The surface charge density σ is given by

$$\sigma = -FC_{A^-}^{\Omega_2} = \frac{-FN_s}{1 + \left(C_{H^+}^0/K_d\right) \exp(-\Phi)}. \quad [14]$$

Therefore, the boundary condition associated with Eq. [4] for case (c) can be expressed as

$$\nabla\Phi \cdot n = \frac{-F^2 N_s D_h}{\varepsilon RT\left[1 + \left(C_{H^+}^0/K_d\right) \exp(-\Phi)\right]}. \quad [15]$$

II.3. Flow Field

Suppose that the spatial variation of the liquid velocity $u(x, y)$ can be described by the Navier–Stokes equation (2)

$$\frac{\partial^2 u}{\partial x^2} + \frac{\partial^2 u}{\partial y^2} = -\frac{[-(\partial p/\partial z) + \rho E_z]}{\eta}, \quad (x, y) \in \Omega. \quad [16]$$

For simplicity, the effect of gravity is neglected in this expression and a body force term ρE_z is included. Equation [16] can be

rewritten in scaled form as

$$\frac{\partial^2 U}{\partial X^2} + \frac{\partial^2 U}{\partial Y^2} = K^2\left[L\frac{G}{a+b} - M\right], \quad [17]$$

where $U = u/u_0$, $L = \varepsilon RT E_z/\eta F u_0$, and $M = P/\eta k^2 u_0$, u_0 being a reference velocity. The boundary conditions associated with Eq. [17] are assumed to be

$$\nabla U \cdot n = 0, \quad (x, y) \in \Omega_1 \text{ or } \Omega_3 \quad [18]$$

$$U = 0, \quad (x, y) \in \Omega_2. \quad [19]$$

Equation [18] arises from the symmetric nature of the problem under consideration, and Eq. [19] states the no-slip condition on the channel wall.

II.4. Electrokinetic Phenomenological Coefficients

In a discussion of the flow through a capillary with a circular cross section Sørensen and Koefoed (3) used the following general relation (21) to characterize an electrokinetic phenomenon,

$$\begin{bmatrix} I_v \\ I_q \end{bmatrix} = \begin{bmatrix} L_{vp} & L_{v\psi} \\ L_{qp} & L_{q\psi} \end{bmatrix} \begin{bmatrix} P \\ E_z \end{bmatrix}, \quad [20]$$

where I_v and I_q are the volumetric flow rate and the electric current, respectively. The elements of the square matrix are the electrokinetic phenomenological coefficients, which are given by (3)

$$L_{vp} = \frac{\pi R_0^4}{8\eta} \quad [21]$$

$$L_{v\psi} = -\frac{2\pi\sigma}{\eta k^3}\Im_{v\psi}(kR_0) \quad [22]$$

$$L_{qp} = -\frac{\pi\sigma}{2\eta k^3}\Im_{qp}(kR_0) \quad [23]$$

$$L_{q\psi} = \frac{2\pi\sigma^2}{\eta k^2}\Im_{q\psi}(kR_0) + \pi\theta^0 R_0^2, \quad [24]$$

where R_0 and θ^0 are, respectively, the radius of the capillary and the specific conductivity. The functions $\Im_{v\psi}(x)$, $\Im_{qp}(x)$, and $\Im_{q\psi}(x)$ are defined as (3)

$$\Im_{v\psi}(x) = x\left[\frac{1}{2}x\frac{I_0(x)}{I_1(x)} - 1\right] \quad [25]$$

$$\Im_{qp}(x) = x^3 - \frac{\int_0^x y^3 I_0(y)\,dy}{I_1(x)} \quad [26]$$

$$\Im_{q\psi}(x) = \frac{1}{I_1(x)}\left[xI_0(x) - \frac{\int_0^x yI_0(y)^2\,dy}{I_1(x)}\right]. \quad [27]$$

In these expressions I_0 and I_1 are the modified Bessel function of the first kind with order zero and that of order one, respectively.

Once the electrical field and the flow field are determined by solving Eqs. [4] and [17] simultaneously subject to the associated boundary conditions, the following expressions can be used to calculate I_v and I_q,

$$I_v = 4\int_\Omega u\,d\Omega, \quad [28]$$

$$I_q = 4\int_\Omega \rho u + [\lambda_a C_a + \lambda_b C_b]E_z\,d\Omega, \quad [29]$$

where λ_m is the molar conductivity of ionic species m, $m = a, b$. The phenomenological coefficients based on the present elliptical microchannel, L'_{vp}, $L'_{v\psi}$, L'_{qp}, and $L'_{q\psi}$, can be calculated based on Eqs. [20], [28], and [29]. To compare the results obtained with the corresponding circular channel, we define the following parameters:

$$\alpha = \frac{L'_{vp}}{L_{vp}} \quad [30]$$

$$\beta = \frac{L'_{v\psi}}{L_{v\psi}} = \frac{L'_{qp}}{L_{qp}} \quad [31]$$

$$\gamma = \frac{L'_{q\psi}}{L_{q\psi}}. \quad [32]$$

Equation [31] is fulfilled under the reciprocity relation of Onsager, which is justified by Sørensen and Koefoed (3).

III. RESULTS AND DISCUSSION

The behavior of the system under consideration is examined through numerical simulation. According to Mala *et al*. (7), the zeta potential of a microchannel can be on the order of 200 mV. The linear size of the microchannels used by Huisman *et al*. (14, 15) and Kemery *et al*. (17) ranged from 0.01 to 0.1 μm, and that of those used by Mala *et al*. (7) ranged from 10 to 100 μm. The magnitudes of the parameters used in our numerical simulations are based on these values. The governing equations are solved by FlexPDE (22) on an IBM PC compatible machine. The applicability of the software used is justified by comparing the numerical values obtained with the theoretical result of Rice and Whitehead (2) in the case of a circular microchannel under the Debye–Hückel condition. It was shown that

$$\frac{\phi}{\phi_0} = \frac{I_0(kr)}{I_0(kD_h/2)} \quad [33]$$

$$u = \frac{P_z}{4\eta}\left(\frac{D_h^2}{4} - r^2\right) - \frac{E_z\varepsilon\phi_0}{\eta}\left[1 - \frac{I_0(kr)}{I_0(kD_h/2)}\right], \quad [34]$$

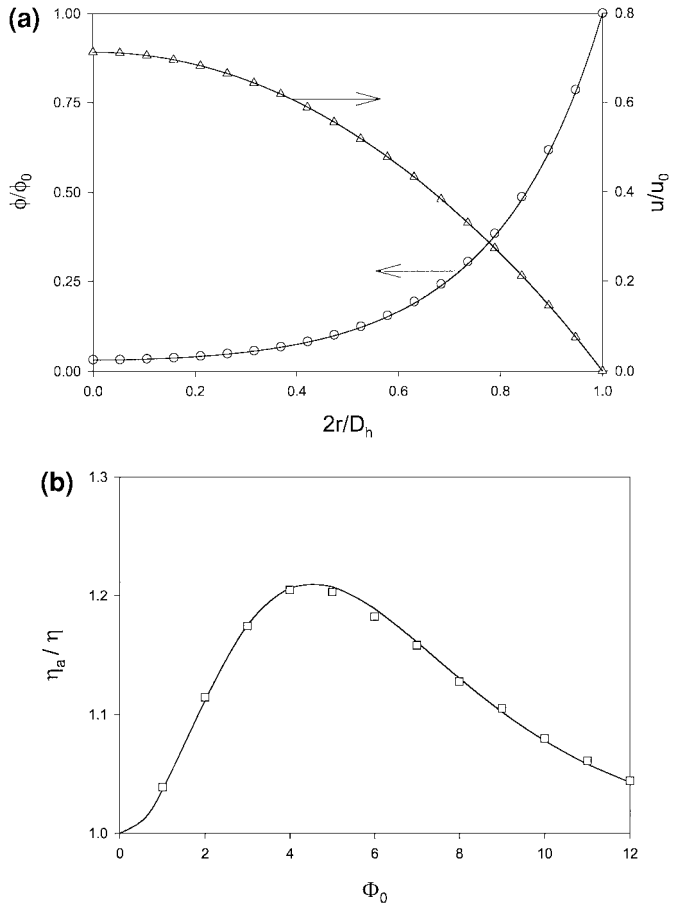

FIG. 2. (a) Variation of both ϕ/ϕ_0 and u/u_0 as a function of scaled radial variable $2r/D_h$ in a circular microchannel. Parameters used are $D_h = 10^{-6}$ m, $I = 10^{-5}$ M, $a = b = 1$, $\phi_0 = -25$ mV, $u_0 = 10^{-3}$ m/s, $T = 298$ K, $\eta = 9 \times 10^{-4}$ kg/m/s, $\varepsilon = 7.0832 \times 10^{-10}$ C/V/m, $P = 10^7$ N/m^3, and $E_z = 1000$ V/m. (b) Variation of η_a/η as a function of Φ_0 in the case of a circular microchannel at $k(D_h/2) = 4$. Parameters used are $a = b = 1$, $T = 298$ K, $\eta = 10^{-3}$ kg/m/s, $\varepsilon = 7.0832 \times 10^{-10}$ C/V/m, and $\lambda_a = \lambda_b = 7.03 \times 10^{-3}$ m^2/ohm/mol. Discrete symbols: (a) analytical result of Rice and Whitehead (2); (b) numerical result of Bowen and Jenner (4); solid lines, present result.

where r and I_0 are, respectively, the radial distance and the modified Bessel function of the first kind of order zero. Figure 2a illustrates the results based on the present study and those evaluated by Eqs. [33] and [34]. The applicability of the numerical scheme adopted in the case of high surface potentials is also examined by comparing our results with those of Bowen and Jenner (4), both are presented in Fig. 2b, which shows the variation of (η_a/η) as a function of Φ_0 at a fixed $k(D_h/2)$ in the case of a circular microchannel. As can be seen from Fig. 2, the performance of the present study is satisfactory.

III.1. Electrical Potential Distribution

Figure 3 shows the distributions of the scaled electrical potential Φ in domain Ω under various boundary conditions. To compare the results based on the three types of electrical boundary conditions on the channel wall, the averaged wall potential,

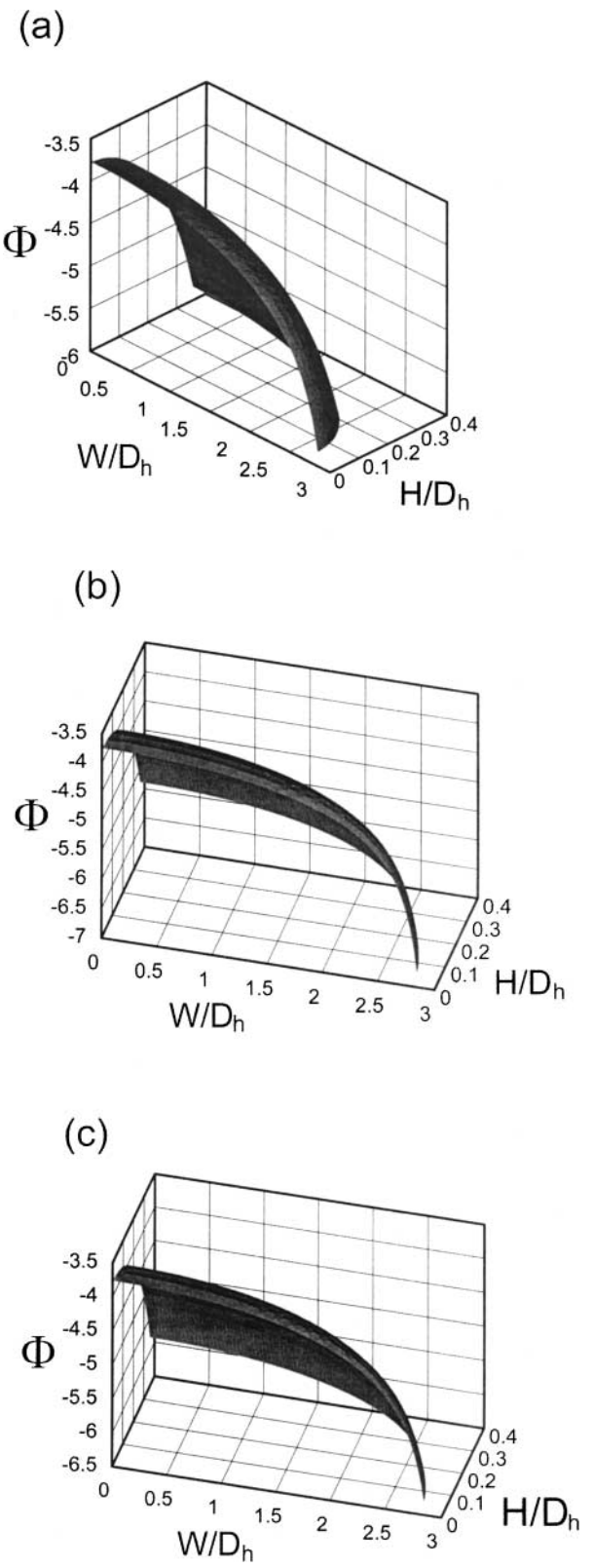

FIG. 3. Distribution of scaled potential Φ in the domain Ω at various boundary conditions. Parameters used are $D_h = 10^{-7}$ m, $I = 10^{-5}$ M, $a = b = 1$, $H/W = 1/8$, $\varepsilon = 7.0832 \times 10^{-10}$ C/V/m, $T = 298$ K, and $\phi_{av} = -150$ mV. (a) Constant surface potential, (b) constant surface charge density, (c) charge-regulated surface.

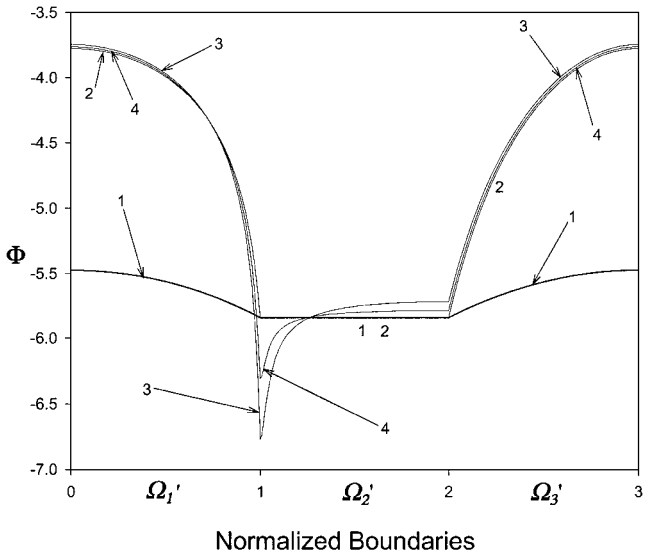

FIG. 4. Variation of scaled potential Φ along the normalized boundaries Ω_1', Ω_2', and Ω_3' for the case in Fig. 3. Curve 1, result based on the Debye–Hückel approximation; Curve 2, constant potential; Curve 3, constant charge density; curve 4, charge-regulated surface.

ϕ_{av}, defined below remains fixed:

$$\phi_{\text{av}} = \frac{1}{\Omega_2}\int_{\Omega_2} \phi \, d\Omega_2. \qquad [35]$$

Note that ϕ_{av} plays the role of the zeta potential. Here, we choose to work on constant ϕ_{av} since the experimentally measured zeta potential represents an averaged surface property. Figure 3 reveals that the difference in Φ based on various types of boundary conditions at the center of a microchannel (i.e., at the origin) is insignificant, but that on the channel wall is appreciable. The latter is because the curvature of the channel wall is position dependent. It can be inferred that the difference in Φ based on various types of boundary conditions on the channel wall disappears as an elliptic channel approaches a circular channel. The variations of Φ along the scaled boundaries Ω_1', Ω_2', and Ω_3', $0 \le \Omega_1' \le 1$, $1 \le \Omega_2' \le 2$, and $2 \le \Omega_3' \le 3$, are presented in Fig. 4. This figure suggests that the largest difference in Φ between various models occurs at the end point of the major axis; that is, $\Omega_1' = \Omega_2' = 1$. As can be seen from Fig. 4, $|\Phi|$ in the case of constant charge density is largest near the point $\Omega_2' = 1$ and is smallest near the point $\Omega_2' = 2$; these apply to the result on the channel wall only. The value of Φ in the case of charge-regulated surface is between that in the case of constant potential and that in the case of constant charge density. For comparison, the distribution of Φ based on the Debye–Hückel approximation in the case of constant potential is also shown in Fig. 4. Note that $|\Phi|$ is overestimated, which is consistent with previous results (6, 8).

III.2. Phenomenological Coefficients

Figure 5 shows the variation of parameters α, β, and γ as a function of the aspect ratio H/W in the case of constant charge

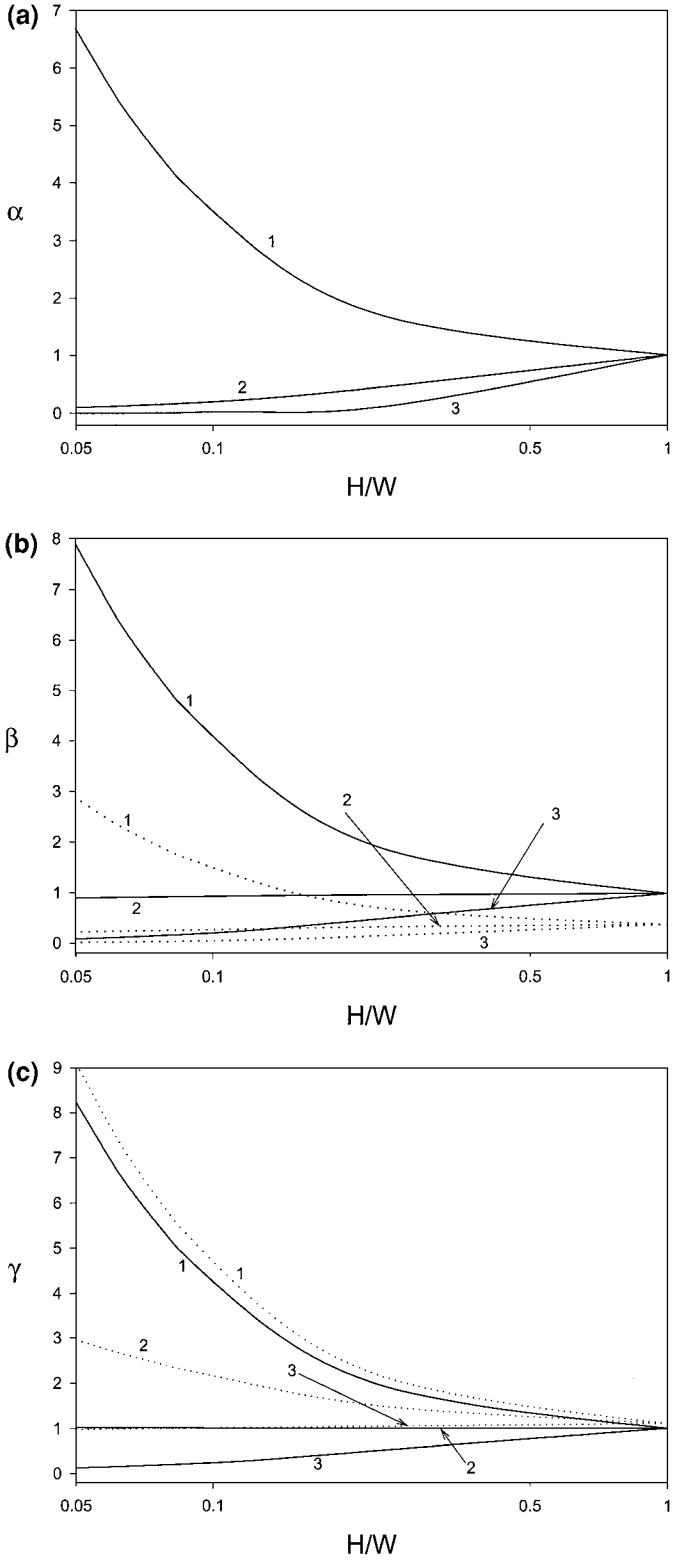

FIG. 5. Variation of parameters α (a), β (b), and γ (c) as a function of the aspect ratio H/W in the case of constant charge density. Solid lines, low charge density, $\sigma = -1.5 \times 10^{-3}$ C/m^2, $I = 10^{-3}$ M; dashed lines, high charge density, $\sigma = -3.0 \times 10^{-3}$ C/m^2, $I = 10^{-5}$ M. Curve 1, fixed hydraulic diameter; Curve 2, fixed cross-sectional area; Curve 3, fixed perimeter. Parameters used are $D_{\text{h}} = 10^{-6}$ m, $a = b = 1$, $\varepsilon = 7.0832 \times 10^{-10}$ C/V/m, $\eta = 9 \times 10^{-4}$ kg/m/s, $T = 298$ K, and $\lambda_a = \lambda_b = 1.546 \times 10^{-2}$ m^2/ohm/mol.

density. Three kinds of constrained situations are considered: constant hydraulic diameter, constant cross-sectional area, and constant perimeter, which depend on the material property or the functional demand of the channel. Note that if $H/W = 1$, a microchannel becomes circular. Figure 5 reveals that in the case of low charge density (solid lines), α, β, and γ all approach unity as $H/W \to 1$. This is consistent with the result of Sørensen and Koefoed (3). On the other hand, in the case of high charge density (dashed lines in Figs. 5b and 5c), both β and γ deviate from unity as $H/W \to 1$; the degree of deviation for the former is larger than that for the latter. This is because the result of Sørensen and Koefoed (3) is based on the Debye–Hückel approximation. In this case, α is a function of hydrodynamic conditions only, as suggested by Eq. [21], and is independent of the charged conditions on the channel wall. Note that $\beta < 1$ and $\gamma > 1$ as $H/W \to 1$; that is, the results of Sørensen and Koefoed (3) overestimate $L_{v\psi}$, but underestimate $L_{q\psi}$. Figure 5a indicates that in the case of fixed hydraulic diameter, α decreases with the increase in H/W, and in the case of fixed cross-sectional area and fixed perimeter, α increases with the increase in H/W. This is because the cross-sectional area of a microchannel decreases with the increase in H/W at a fixed hydraulic diameter. It is apparent that this effect reduces the volumetric flow rate as H/W increases, and so does α. Another factor we should consider is the effect of wall viscous retardation, which arises from the no-slip boundary condition and the viscous property of the liquid phase. If H/W decreases, the channel becomes narrow, the effect of wall viscous retardation increases, and the flow of fluid is retarded. Figure 5a (curve 1) suggests that as H/W decreases, the effect of wall viscous retardation is weaker than that of increasing the cross-sectional area. If the cross-sectional area is fixed, the effect of wall viscous retardation plays the major role, and therefore α increases with the increase in H/W. If the perimeter is fixed, the cross-sectional area increases with the increase in H/W and the wall viscous retardation decreases with the increase in H/W. Therefore α increases with the increase in H/W. Figure 5a also suggests that, for fixed H/W, the magnitude of α follows the order (fixed hydraulic diameter)>(fixed cross sectional area)>(fixed perimeter). Figure 5b reveals that the qualitative behavior of β as H/W varies is similar to that of α and can be explained by similar reasoning. However, the value of β for fixed cross-sectional area only slightly increases with the increase in H/W. This implies that the effect of fluid flow on the deformation of the electric double layer is comparable to that on wall viscous retardation; these two effects have an opposite contribution to fluid flow. The qualitative behavior of γ shown in Fig. 5c is similar to that of α shown in Fig. 5a except in the case of fixed cross-sectional area, in which γ decreases with the increase in H/W. Also, the higher the charge density the faster the rate of decrease in γ as H/W increases. This implies that the effect of the deformation of the electric double layer on the electric current is more significant than that of wall viscous retardation. The results shown in Fig. 5 indicate that the cross-sectional area of a microchannel plays a dominant role in the electrokinetic phenomenon under consideration.

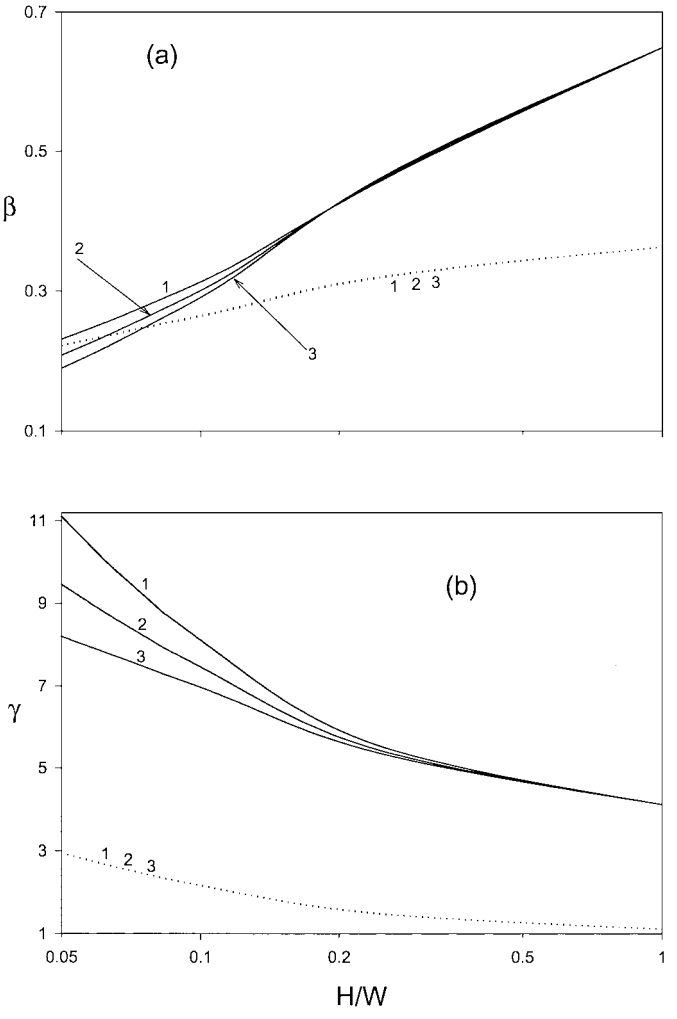

FIG. 6. Variation of parameters β (a) and γ (b) as a function of the aspect ratio H/W in the case of a constant-cross sectional area. Solid lines, $D_h = 10^{-7}$ m; dashed lines $D_h = 10^{-6}$ m. Curve 1, constant charge density with $\sigma = -3.0 \times 10^{-3}$ C/m^2. Curve 2, charge-regulated surface with pH 7 and $K_d = 10^{-5}$ M, $N_s = 1.150 \times 10^{-7}$ mol/m^2 for $D_h = 10^{-6}$ m and $N_s = 1.495 \times 10^{-7}$ mol/m^2 for $D_h = 10^{-6}$ m. Curve 3, constant potential with $\phi_0 = -143.724$ mV for $D_h = 10^{-7}$ m and $\phi_0 = -152.585$ mV for $D_h = 10^{-7}$ m. Parameters used are $I = 10^{-5}$ M, $a = b = 1$, $\varepsilon = 7.0832 \times 10^{-10}$ C/V/m, $\eta = 9 \times 10^{-4}$ kg/m/s, $T = 298$ K, and $\lambda_a = \lambda_b = 1.546 \times 10^{-2}$ m^2/ohm/mol.

Figure 6 shows the variation of the parameters β and γ as a function of the aspect ratio H/W in the case of a constant cross-sectional area under various surface conditions at two different hydraulic diameters. A cylindrical microchannel (i.e., $H/W = 1$) with a fixed charge density is used as the basis in the numerical calculations. For example, let us consider the case when $D_h = 10^{-6}$ m and $\sigma = -3.0 \times 10^{-3}$ C/m^2. The surface potential of the corresponding constant surface potential model is estimated as $\phi_0 = -143.724$ mV, and the parameters of the corresponding charge-regulated surface are evaluated as pH 7, $K_d = 10^{-5}$ M, and $N_s = 1.150 \times 10^{-7}$ mol/m^2. Then β and γ at various H/W are based on these values. This figure suggests that if the hydraulic diameter is large, the results based on different

surface conditions are essentially the same. On the other hand, if the hydraulic diameter is small, the difference becomes appreciable, and the smaller the H/W the larger the difference. Figure 6 reveals that the constant charge density model yields the largest β and γ, and the constant potential model gives the smallest β and γ. Also, the deviation of the result of Sørensen and Koefoed (3) is smaller for β and larger for γ in the case of smaller hydraulic diameter (i.e., at $H/W = 1$, β is closer to unity than γ is).

III.3. Electrokinetic Parameters

The values of α, β, and γ are readily applicable to the estimation of the key components of the present electrokinetic phenomenon, for example, electroosmotic volumetric flow rate, $I_{\rm vo}$, streaming potential, $E_{\rm st}$, total electric current, $I_{\rm q}$, and electroviscous effect. The last component is measured by the ratio $I_{\rm vr}/I_{\rm vp}$, which is also adopted by Burgreen and Nakache (1), $I_{\rm vr}$ being the retarding volumetric flow rate and $I_{\rm vp}$ the pressure-induced volumetric flow rate. These components can be evaluated based on Eq. [20] as

$$I_{\rm vo} = \beta L_{\rm v\psi} E_z \qquad [36]$$

$$E_{\rm st} = -\frac{\beta L_{\rm qp}}{\gamma L_{\rm q\psi}} P \qquad [37]$$

$$I_{\rm q} = \beta L_{\rm qp} P + \gamma L_{\rm q\psi} E_z \qquad [38]$$

$$I_{\rm vr}/I_{\rm vp} = \frac{\beta^2 L_{\rm v\psi} L_{\rm qp}}{\alpha\gamma L_{\rm q\psi} L_{\rm vp}}. \qquad [39]$$

The behaviors of these components under three kinds of constraint as the aspect ratio varies can be inferred easily on the basis of the variations of α, β, and γ shown in Fig. 5. For example, for a fixed cross-sectional area of a microchannel, both the electroosmotic volumetric flow rate $I_{\rm vo}$ and the absolute streaming potential $|E_{\rm st}|$ increase monotonically with the increase in the aspect ratio H/W, as shown in Fig. 7. This can be explained as follows. As indicated in Fig. 5, β increases with the increase in H/W but γ varies oppositely, and therefore β/γ increases with the increase in H/W. According to Eqs. [36] and [37], $I_{\rm vo}$ and $|E_{\rm st}|$ are proportional to β and β/γ, respectively, and the results shown in Fig. 7 are expected.

Figure 8 shows the variation of the total electric current $I_{\rm q}$ as a function of the aspect ratio H/W in the case of a constant cross-sectional area at two levels of wall potential. This figure reveals that the total electric current may have a local minimum as H/W varies. According to Eq. [38], the total electric current is made up of both the applied electrical field and the applied pressure gradient. Since the proportional coefficients of these two factors, β and γ, vary oppositely as the aspect ratio varies, as shown in Fig. 5, the total electric current may have a local minimum as the aspect ratio varies.

The variation of the ratio $I_{\rm vr}/I_{\rm vp}$ as a function of the aspect ratio H/W in the case of a constant cross-sectional area at constant charge density is presented in Fig. 9. As mentioned previously, $I_{\rm vr}/I_{\rm vp}$ is a measure for the magnitude of electroviscous effect. Figure 9 reveals that the qualitative behavior of $I_{\rm vr}/I_{\rm vp}$ as H/W varies depends on the magnitude of the hydraulic diameter. If $D_{\rm h}$ is large, $I_{\rm vr}/I_{\rm vp}$ decreases with the increase in H/W, and the inverse is true if it is small. Therefore, $I_{\rm vr}/I_{\rm vp}$ may have a local minimum as H/W varies at a certain hydraulic diameter. This can be explained by Eq. [39]. As indicated in Fig. 5, both α and β increase with the increase in H/W and γ varies oppositely; therefore, $\beta^2/\alpha\gamma$ may have a local extrema, so does $I_{\rm vr}/I_{\rm vp}$.

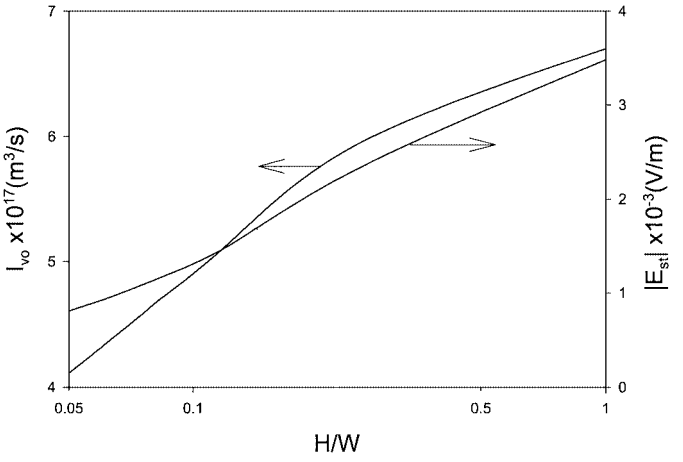

FIG. 7. Variation of electroosmotic volumetric flow rate $I_{\rm vo}$ ($P = 0$, $E = 1000$ V/m) and absolute streaming potential $|E_{\rm st}|$($P = 10^8$ N/m^3, $E = 0$) as a function of the aspect ratio H/W in the case of a constant cross-sectional area and a constant potential. Parameters used are $\phi_0 = -143.724$ mV, $D_{\rm h} = 10^{-6}$ m, $I = 10^{-5}$ M, $a = b = 1$, $T = 298$ K, $\varepsilon = 7.0832 \times 10^{-10}$ C/V/m, $\eta = 9 \times 10^{-4}$ kg/m/s, and $\lambda_a = \lambda_b = 1.546 \times 10^{-2}$ m^2/ohm/mol.

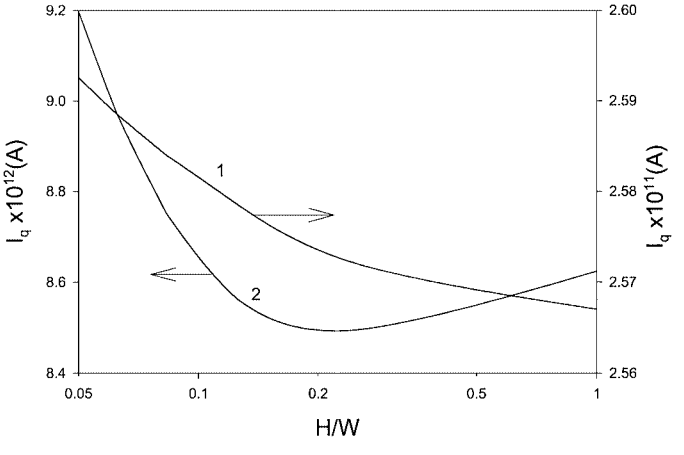

FIG. 8. Variation of total electric current $I_{\rm q}$ as a function of the aspect ratio H/W in the case of a constant cross-sectional area and constant potential. Curve 1, $\phi_0 = -20.220$ mV and $I = 10^{-3}$ M, Curve 2, $\phi_0 = -143.724$ mV, and $I = 10^{-5}$ M. Parameters used are $P = 10^8$ N/m^3, $E = 1000$ V/m, $D_{\rm h} = 10^{-6}$ m, $a = b = 1$, $\varepsilon = 7.0832 \times 10^{-10}$ C/V/m, $\eta = 9 \times 10^{-4}$ kg/m/s, $T = 298$ K, and $\lambda_a = \lambda_b = 1.546 \times 10^{-2}$ m^2/ohm/mol.

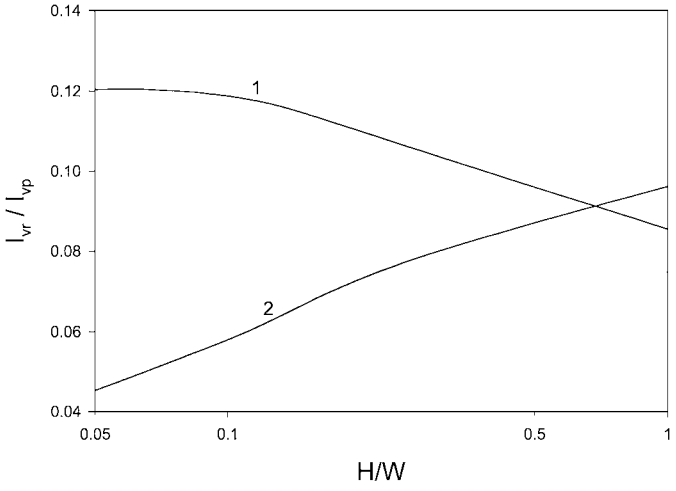

FIG. 9. Variation of I_{vr}/I_{vp} as a function of the aspect ratio H/W in the case of a constant cross-sectional area and a constant charge density. Curve 1, $D_h = 10^{-6}$ m, curve 2, $D_h = 10^{-7}$ m. Parameters used are $\sigma = -3.0 \times 10^{-3}$ C/m^2, $I = 10^{-5}$ M, $a = b = 1$, $\varepsilon = 7.0832 \times 10^{-10}$ C/V/m, and $\eta = 9 \times 10^{-4}$ kg/m/s, $T = 298$ K, and $\lambda_a = \lambda_b = 1.546 \times 10^{-2}$ m^2/ohm/mol.

IV. CONCLUSION

The electrokinetic phenomenological coefficients for the flow of an electrolyte solution through an elliptical microchannel are evaluated. In particular, their variations as a function of the aspect ratio of the microchannel at constant hydraulic diameter, constant cross-sectional area, or constant perimeter of the microchannel are investigated. Three types of boundary conditions on the channel wall are considered, which include constant surface charge, constant surface potential, and charge-regulated surface. It is found that the smaller the size of a microchannel the more apparent the difference between the results based on these boundary conditions. We show that, as the aspect ratio varies, the electroosmotic volumetric flow rate, the streaming potential, the total electric current, and the electroviscous effect can easily be evaluated through three basic parameters.

ACKNOWLEDGMENT

This work is supported by the National Science Council of the Republic of China.

REFERENCES

1. Burgreen, D., and Nakache, F. R., *J. Phys. Chem.* **68,** 1084 (1964).
2. Rice, C. L., and Whitehead, R., *J. Phys. Chem.* **69,** 4017 (1965).
3. Sørensen, T. S., and Koefoed, J., *J. Chem. Soc. Faraday Trans. 2* **70,** 665 (1974).
4. Bowen, W. R., and Jenner, F., *J. Colloid Interface Sci.* **173,** 388 (1995).
5. Mala, G. M., Li, D., and Dale, J. D., *Int. J. Heat Mass Transfer* **40,** 3079 (1997).
6. Qian, Y., Yang, G., and Bowen, W. R., *J. Colloid Interface Sci.* **190,** 55 (1997).
7. Mala, G. M., Li, D., Werner, C., Jacobasch, H. J., and Ning, Y. B., *Int. J. Heat Fluid Flow* **18,** 489 (1997).
8. Mala, G. M., Yang, C., and Li, D., *Colloids Surf. A* **135,** 109 (1998).
9. Yang, C., and Li, D., *J. Colloid Interface Sci.* **194,** 95 (1997).
10. Yang, C., and Li, D., *Colloids Surf. A* **143,** 339 (1998).
11. Yang, C., Li, D., and Masliyah, J. H., *Int. J. Heat Mass Transfer* **41,** 4229 (1998).
12. Mala, G. M., and Li, D., *Int. J. Heat Fluid Flow* **20,** 142 (1999).
13. Weilin, Q., Mala, G. M., and Li, D., *Int. J. Heat Mass Transfer* **43,** 353 (2000).
14. Huisman, I. H., Pradanos, P., and Hernandez, A., *J. Membr. Sci.* **178,** 55 (2000).
15. Huisman, I. H., Pradanos, P., Calvo, J. I., and Hernandez, A., *J. Membr. Sci.* **178,** 79 (2000).
16. Ren, L., Li, D., and Weilin, Q., *J. Colloid Interface Sci.* **233,** 12 (2001).
17. Kemery, P. J., Steehler, J. K., and Bohn, P. W., *Langmuir* **14,** 2884 (1998).
18. Coelho, D., Shapiro, M., Thovert, J. F., and Adler, P. M., *J. Colloid Interface Sci.* **181,** 169 (1996).
19. Ohshima, H., and Kondo, T., *J. Colloid Interface Sci.* **135,** 443 (1990).
20. Spiegel, M. S., "Mathematical Handbook of Formulas and Tables," McGraw–Hill, New York, 1968.
21. De Groot, S. R., and Mazur, P., "Non-equilibrium Thermodynamics," North-Holland, Amsterdam, 1962.
22. FlexPDE, Version 2.22, PDE Solutions Inc., USA.